Imaging of the CO Snow Line in a Solar Nebula Analog

Chunhua Qi *et al.*

Science **341**, 630 (2013);
DOI: 10.1126/science.1239560

Science (print ISSN 0036-8075; online ISSN 1095-9203) is published weekly, except the last week in December, by the American Association for the Advancement of Science, 1200 New York Avenue NW, Washington, DC 20005.

Imaging of the CO Snow Line in a Solar Nebula Analog

Chunhua Qi,[1]*† Karin I. Öberg,[2]*‡ David J. Wilner,[1] Paola D'Alessio,[3] Edwin Bergin,[4] Sean M. Andrews,[1] Geoffrey A. Blake,[5] Michiel R. Hogerheijde,[6] Ewine F. van Dishoeck[6,7]

Planets form in the disks around young stars. Their formation efficiency and composition are intimately linked to the protoplanetary disk locations of "snow lines" of abundant volatiles. We present chemical imaging of the carbon monoxide (CO) snow line in the disk around TW Hya, an analog of the solar nebula, using high spatial and spectral resolution Atacama Large Millimeter/Submillimeter Array observations of diazenylium (N_2H^+), a reactive ion present in large abundance only where CO is frozen out. The N_2H^+ emission is distributed in a large ring, with an inner radius that matches CO snow line model predictions. The extracted CO snow line radius of ~30 astronomical units helps to assess models of the formation dynamics of the solar system, when combined with measurements of the bulk composition of planets and comets.

Condensation fronts in protoplanetary disks, where abundant volatiles deplete out of the gas phase and are incorporated into solids, are believed to have played a critical role in the formation of planets in the solar system (*1*, *2*), and similar "snow lines" in the disks around young stars should affect the ongoing formation of exoplanets. Snow lines can enhance particle growth and thus planet formation efficiencies because of (i) substantial increases in solid mass surface densities exterior to snow line locations, (ii) continuous freeze-out of gas diffusing across the snow line (cold-head effect), (iii) pile-up of dust just inside of the snow line in pressure traps, and (iv) an increased "stickiness" of icy grains compared with bare ones, which favors dust coagulation (*3*–*7*). Experiments and theory on these processes have been focused on the H_2O snow line, but the results should be generally applicable to snow lines of abundant volatiles, with the exception that the stickiness of different icy grain mantles varies. The locations of snow lines of the most abundant volatiles—H_2O, CO_2, and CO—with respect to the planet-forming zone may also regulate the bulk composition of planets (*8*). Determining snow line locations is therefore key to probing grain growth—and thus, planetesimal and planet formation efficiencies—and elemental and molecular compositions of planetesimals and planets forming in protoplanetary disks, including the solar nebula.

According to the solar system's composition and disk theory, the H_2O snow line developed at ~3 astronomical units (AU, where 1 AU is the average distance from the Earth to the Sun) from the early Sun during the epoch of chondrite assembly (*9*). In other protoplanetary disks, the snow line locations are determined by the disk midplane temperature structures, which are set by a time-dependent combination of the luminosity of the central star, the presence of other heating sources, the efficiencies of dust and gas cooling, and the intrinsic condensation temperatures of different volatiles. Because of the low condensation temperature of CO, the CO snow line occurs at radii of tens of AU around solar-type stars: this larger-sized scale makes the CO transition zone the most accessible to direct observations. The CO snow line is also important in its own right because CO ice is a starting point for a complex, prebiotic chemistry (*10*). Also, without incorporating an enhanced grain growth efficiency beyond that expected for bare silicate dust, observations of centimeter-sized dust grains in disks, including in TW Hya (*11*), are difficult to reproduce in the outer disk. Condensation of CO is very efficient below the CO freeze-out temperature, with a sticking efficiency close to unity according to experiments (*12*), and a CO condensation–based dust growth mode may thus be key to explaining these observations.

Protoplanetary disks have evolving radial and vertical temperature gradients, with a warmer surface where CO remains in the gaseous state throughout the disk, even as it is frozen in the cold, dense region beyond the midplane snow line (*13*). This means that the midplane snow line important for planet formation constitutes a smaller portion of a larger condensation surface. Because the bulk of the CO emission comes from the disk surface layers, this presents a challenge for locating the CO midplane snow line. Its location has been observationally identified toward only one system, the disk around HD 163296, based on millimeter (or sub-millimeter) interferometric observations of multiple CO rotational transitions and isotopologues at high spatial resolution, interpreted through detailed modeling of the disk dust and gas physical structure (*14*). An alternative approach to constrain the CO snow line, suggested in (*15*) and pursued here, is to image molecular emission from a species that is abundant only where CO is highly depleted from the gas phase.

N_2H^+ emission is expected to be a robust tracer of CO depletion because the presence of gas phase CO both slows down N_2H^+ formation and speeds up N_2H^+ destruction. N_2H^+ forms through reactions between N_2 and H_3^+, but most H_3^+ will instead transfer a proton to CO as long as the more abundant CO remains in the gas phase. The most important destruction mechanism for N_2H^+ is proton transfer to a CO molecule, whereas

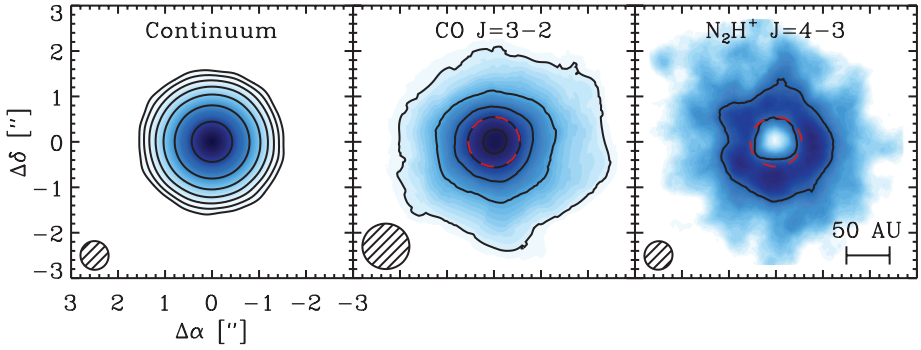

Fig. 1. Observed images of dust, CO, and N_2H^+ emission toward TW Hya. (**Left**) ALMA 372-GHz continuum map, extracted from the line-free channels of the N_2H^+ observations. Contours mark [5, 10, 20, 40, 80, 160, 320] millijansky (mJy) beam^{-1}, and the root mean square (RMS) is 0.2 mJy beam^{-1}. (**Center**) Image of CO J = 3–2 emission acquired with the SMA (*24*). Contours mark (*1*–*5*) Jy km s^{-1} beam^{-1}, and the RMS is 0.1 Jy km s^{-1} beam^{-1}. (**Right**) ALMA image of N_2H^+ J = 4–3 integrated emission with a single contour at 150 mJy km s^{-1} beam^{-1}, and the RMS is 10 mJy km s^{-1} beam^{-1}. The synthesized beam sizes are shown in each bottom left corner. The red dashed circle marks the best-fit inner radius of the N_2H^+ ring from a modeling of the visibilities. This inner edge traces the onset of CO freeze-out according to astrochemical theory and thus marks the CO snow line in the disk midplane.

[1]Harvard-Smithsonian Center for Astrophysics, Cambridge, MA 02138, USA. [2]Departments of Chemistry and Astronomy, University of Virginia, Charlottesville, VA 22904, USA. [3]Centro de Radioastronomõa y Astrofisica, Universidad Nacional Autonoma de Mexico (UNAM), 58089 Mexico City, Mexico. [4]Department of Astronomy, University of Michigan, Ann Arbor, MI 48109, USA. [5]Division of Geological and Planetary Sciences, California Institute of Technology, Pasadena, CA 91125, USA. [6]Leiden Observatory, Leiden University, 2300 RA Leiden, Netherlands. [7]Max Planck Institute for Extraterrestrial Physics, 85748 Garching, Germany.
*These authors contributed equally to this work.
†Corresponding author. E-mail: cqi@cfa.harvard.edu
‡Present address: Harvard-Smithsonian Center for Astrophysics, Cambridge, MA 02138, USA.

in the absence of CO, N_2H^+ is destroyed through a much slower dissociative recombination reaction. These simple astrochemical considerations predict a correlation between N_2H^+ and CO depletion, or equivalently an anticorrelation between N_2H^+ and gas-phase CO. The latter has been observed in many prestellar and protostellar environments, confirming the basic theory (*16*, *17*). In disks, N_2H^+ should therefore be present at large abundances only inside the vertical and horizontal thermal layers where CO vapor is condensing—that is, beyond the CO snow line. Molecular line surveys of disks have shown that N_2H^+ is only present in disks cold enough to entertain CO freeze-out (*18*), and marginally resolved observations hint at a N_2H^+ emission offset from the stellar position (*15*), which is in agreement with the models of disk chemistry (*19*). Detailed imaging of N_2H^+ emission in protoplanetary disks at the scales needed to directly reveal CO snow lines with sufficient sensitivity has previously been out of reach.

We used the Atacama Large Millimeter/Submillimeter Array (ALMA) to obtain images of emission from the 372-GHz dust continuum and the N_2H^+ $J = 4 - 3$ rotational line (where J is the rotational quantum number) from the disk around TW Hya (Fig. 1 and fig. S1) (*20*). TW Hya is the closest (54 ± 6 pc) and as such is the most intensively studied pre–main-sequence star with a gas-rich circumstellar disk (*21*, *22*). According to previous observations of dust and CO emission, and the recent detection of HD line emission (*23*), this 3 million– to 10 million–year-old, 0.8 solar mass ($M_\odot$) T Tauri star (spectral type K7) is known to be surrounded by an almost face-on (~6° inclination) massive ~0.04 $M_\odot$ gas-rich disk. The disk size in millimeter dust is ~60 AU, with a more extended (>100 AU) disk in gas and micrometer-sized dust (*24*). Both the disk mass and size conform well with solar nebula estimates—the minimum mass of the solar nebula is 0.01 $M_\odot$, based on planet masses and compositions (*9*)—and the disk around TW Hya may thus serve as a template for planet formation in the solar nebula. Our images show that N_2H^+ emission is distributed in a ring with an inner diameter of 0.8 to 1.2 arc sec (based on visual inspection), corresponding to a physical inner radius of 21 to 32 AU. In contrast, CO emission is detected down to radial scales of ~2 AU (*25*). The clear difference in morphology between the N_2H^+ and CO emission can be simply explained by the presence of a CO midplane snow line at the observed inner edge of the N_2H^+ emission ring. The different morphologies cannot be explained by a lack of ions in the inner disk, based on previous spatially and spectrally resolved observations of another ion, HCO^+ (*22*). These HCO^+ observations had lower sensitivity and angular resolution than those of the N_2H^+ observations, but they are sufficient to exclude a central hole comparable in size with that seen in N_2H^+.

To associate the inner-edge radius of the N_2H^+ emission with a midplane temperature, and thus a CO freeze-out temperature, requires a model of the disk density and temperature structure. We adopted the model presented in (*22*), updated to conform with recent observations of the accretion rate and grain settling (figs. S2 to S4 and table S1) (*20*). In the context of this disk structure model, the N_2H^+ inner-edge location implies that N_2H^+ becomes abundant where the midplane temperature drops to 16 to 20 K. This is in agreement with expectations for the CO freeze-out temperature on the basis of the outcome of the laboratory experiments and desorption modeling by (*12*), who found CO condensation/sublimation temperatures of 16 to 18 K under interstellar conditions, assuming heat-up rates of 1 K per 10^2 to 10^6 years. In outer-disk midplanes, condensation temperatures are expected to be at most a few degrees higher because of a weak dependence on density (*26*). If CO condenses onto H_2O ice rather than existing CO ice, the condensation temperature will increase further, but this will only affect the first few monolayers of ice and is not expected to change the location where the majority of CO freezes out. Some CO may also remain in the gas phase below the CO freeze-out temperature in the presence of efficient nonthermal desorption, especially ultraviolet (UV) photodesorption (*27*), but this is expected to be negligible in the disk midplane at 30 AU because of UV shielding by upper-disk layers. UV photodesorption may affect the vertical CO snow surface location, however, and thus, describing the radial and vertical condensation surfaces with a single freeze-out temperature may not be possible.

To locate the inner edge of the N_2H^+ ring more quantitatively, we simulated the N_2H^+ emission with a power-law column density distribution and compared this with the data. We assumed the disk material orbits the central star in Keplerian motion and fixed the geometric and kinematic parameters of the disk that affect its observed spatio-kinematic behavior (*22*). We used the same updated density and temperature disk structure model (*20*) and assumed that the N_2H^+ column density structure could be approximated as a radial power law with inner and outer edges, whereas vertically the abundance was taken to be constant between the lower (toward midplane) and upper (toward surface) boundaries. This approach crudely mimics the results of detailed astrochemical modeling of disks, which shows that molecules are predominantly present in well-defined vertical layers (*13*, *19*), and has been used to constrain molecular abundance structures in a number of previous studies (*15*, *22*). The inner and outer radii, power-law index, and column density at 100 AU were treated as free parameters. We calculated a grid of synthetic N_2H^+ visibility data sets using the RATRAN code (*28*) to determine the radiative transfer and molecular excitation and compared them with the N_2H^+ observations. We obtained the best-fit model by minimizing χ^2, the weighted difference between the data and the model with the real and imaginary part of the

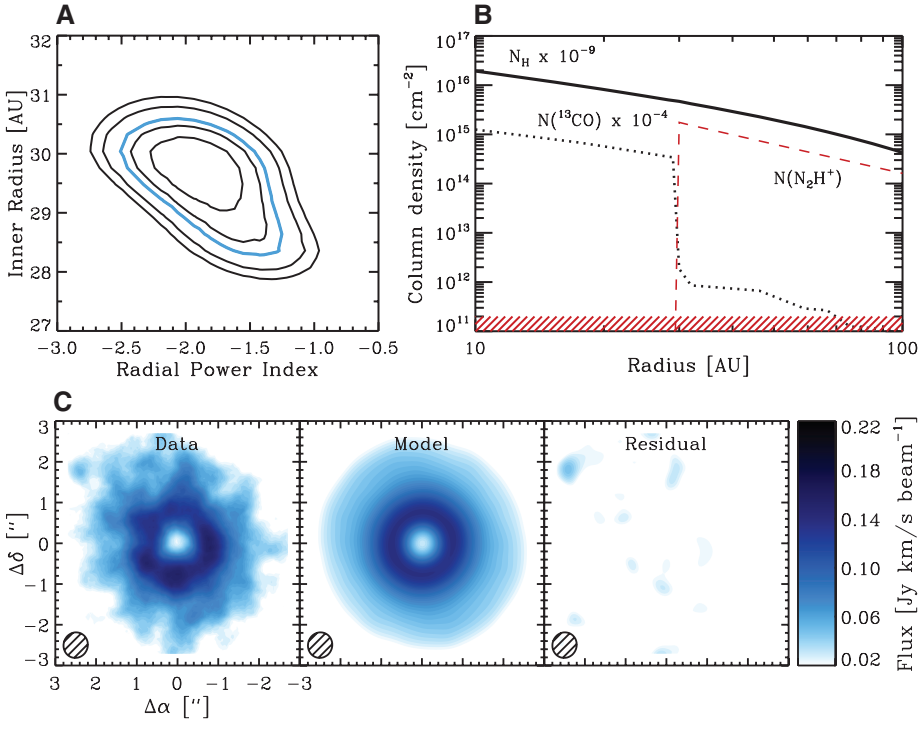

Fig. 2. Model results for the N_2H^+ abundance structure toward TW Hya. (**A**) The χ^2 fit surface for the power-law index and inner radius of the N_2H^+ abundance profile. Contours correspond to the 1σ to 5σ errors, and the blue contour marks 3σ. (**B**) The best-fit N_2H^+ column density structure, shown together with the total gas column density and the best-fit ^{13}CO column density for CO freeze-out at 17 K. The shaded region marks the N_2H^+ 1σ detection limit. (**C**) N_2H^+ observations, simulated observations of the best-fit N_2H^+ model, and the imaged residuals, calculated from the visibilities.

complex visibility measured in the (u,v) plane sampled by the ALMA observations of N_2H^+.

As demonstrated in Fig. 2A, the inner radius is well constrained to 28 to 31 AU (3σ). This edge determination was aided by the nearly face-on viewing geometry because this minimizes the impact of the detailed vertical structure on the disk-modeling outcome. Furthermore, the Keplerian kinematics of the gas help to constrain the size scale at a level finer than the spatial resolution implied by the synthesized beam size. As a result, the fitted inner radius is robust to the details of the density and temperature model (table S2) (*20*). In the context of this model, the best-fit N_2H^+ inner radius corresponds to a CO midplane snow line at a temperature of 17 K. The best-fit N_2H^+ column density profile is presented in Fig. 2B together with the best-fit ^{13}CO profile, assuming a CO freeze-out temperature of 17 K (*20*) (fig. S5 and table S3). We fit ^{13}CO emission [obtained with the Submillimeter Array (*20*)] because the main isotopologue CO lines are optically thick. The N_2H^+ column density contrast across the CO snow line is at least an order of magnitude (*20*). Simulated ALMA observations of the best-fit N_2H^+ $J = 4–3$ model are shown in Fig. 2C, demonstrating the excellent agreement.

Our quantitative analysis thus confirms the predictions that N_2H^+ traces the snow line of the abundant volatile, CO. Furthermore, the agreement between the quantitative analysis and the visual estimate of the N_2H^+ inner radius demonstrates that N_2H^+ imaging is a powerful tool to determine the CO snow line radii in disks, whose density and temperature structures have not been modeled in detail. N_2H^+ imaging with ALMA may therefore be used to provide statistics on how snow line locations depend on parameters of interest for planet formation theory, such as the evolutionary stage of the disks.

The locations of snow lines in solar nebula analogs such as TW Hya are also important to understand the formation dynamics of the solar system. The H_2O snow line is key to the formation of Jupiter and Saturn (*29*), whereas CH_4 and CO freeze-out enhanced the solid surface density further out in the solar nebula, which may have contributed to the feeding zones of Uranus and Neptune (*30*), depending on exactly where these ice giants formed. In the popular Nice model for the dynamics of the young solar system, Uranus formed at the largest radius of all planets, at ~17 AU (*31*), and most comets and Kuiper Belt objects formed further out, to ~35 AU. The plausibility of this scenario can be assessed by using the bulk compositions of these bodies together with knowledge of the CO snow line location. In particular, Kuiper Belt objects contain CO and the even more volatile N_2 (*32*, *33*), which implies that they must have formed beyond the CO snow line. Comets exhibit a range of CO abundances, some of which seem to be primordial, which suggests that the CO snow line was located in the outer part of their formation region of 15 to 35 AU (*34*). This is consistent with the CO snow line radius that we have determined in the TW Hya disk. However, in the context of the Nice model this CO snow line radius is too large for the ice giants and suggests that their observed carbon enrichment has a different origin than the accretion of CO ice (*30*). A caveat is that H_2O ice can trap CO, although this process is unlikely to be efficient enough to explain the observations. In either case, the CO snow line locations in solar nebula analogs such as TW Hya offer independent constraints on the early history of the solar system.

References and Notes

1. J. S. Lewis, *Science* **186**, 440–443 (1974).
2. D. J. Stevenson, J. I. Lunine, *Icarus* **75**, 146–155 (1988).
3. F. J. Ciesla, J. N. Cuzzi, *Icarus* **181**, 178–204 (2006).
4. A. Johansen *et al.*, *Nature* **448**, 1022–1025 (2007).
5. E. Chiang, A. N. Youdin, *Annu. Rev. Earth Planet. Sci.* **38**, 493–522 (2010).
6. B. Gundlach, S. Kilias, E. Beitz, J. Blum, *Icarus* **214**, 717–723 (2011).
7. K. Ros, A. Johansen, *Astron. Astrophys.* **552**, A137 (2013).
8. K. I. Öberg, R. Murray-Clay, E. A. Bergin, *Astrophys. J.* **743**, L16 (2011).
9. C. Hayashi, *Prog. Theor. Phys.* **70** (suppl.), 35–53 (1981).
10. E. Herbst, E. F. van Dishoeck, *Annu. Rev. Astron. Astrophys.* **47**, 427–480 (2009).
11. D. J. Wilner, P. D'Alessio, N. Calvet, M. J. Claussen, L. Hartmann, *Astrophys. J.* **626**, L109–L112 (2005).
12. S. E. Bisschop, H. J. Fraser, K. I. Öberg, E. F. van Dishoeck, S. Schlemmer, *Astron. Astrophys.* **449**, 1297–1309 (2006).
13. Y. Aikawa, E. Herbst, *Astron. Astrophys.* **351**, 233 (1999).
14. C. Qi *et al.*, *Astrophys. J.* **740**, 84 (2011).
15. C. Qi, K. I. Öberg, D. J. Wilner, *Astrophys. J.* **765**, 34 (2013).
16. E. A. Bergin, J. Alves, T. Huard, C. J. Lada, *Astrophys. J.* **570**, L101–L104 (2002).
17. J. K. Jørgensen, *Astron. Astrophys.* **424**, 589 (2004).
18. K. I. Öberg *et al.*, *Astrophys. J.* **734**, 98 (2011).
19. C. Walsh, H. Nomura, T. J. Millar, Y. Aikawa, *Astrophys. J.* **747**, 114 (2012).
20. Materials and methods are available as supplementary materials on *Science* Online.
21. J. H. Kastner, B. Zuckerman, D. A. Weintraub, T. Forveille, *Science* **277**, 67–71 (1997).
22. C. Qi, D. J. Wilner, Y. Aikawa, G. A. Blake, M. R. Hogerheijde, *Astrophys. J.* **681**, 1396–1407 (2008).
23. E. A. Bergin *et al.*, *Nature* **493**, 644–646 (2013).
24. S. M. Andrews *et al.*, *Astrophys. J.* **744**, 162 (2012).
25. K. A. Rosenfeld *et al.*, *Astrophys. J.* **757**, 129 (2012).
26. D. Hollenbach, M. J. Kaufman, E. A. Bergin, G. J. Melnick, *Astrophys. J.* **690**, 1497–1521 (2009).
27. K. Willacy, *Astrophys. J.* **660**, 441–460 (2007).
28. M. R. Hogerheijde, F. F. S. van der Tak, *Astron. Astrophys.* **362**, 697 (2000).
29. M. Lecar, M. Podolak, D. Sasselov, E. Chiang, *Astrophys. J.* **640**, 1115–1118 (2006).
30. S. E. Dodson-Robinson, K. Willacy, P. Bodenheimer, N. J. Turner, C. A. Beichman, *Icarus* **200**, 672–693 (2009).
31. K. Tsiganis, R. Gomes, A. Morbidelli, H. F. Levison, *Nature* **435**, 459–461 (2005).
32. T. C. Owen *et al.*, *Science* **261**, 745–748 (1993).
33. S. C. Tegler *et al.*, *Astrophys. J.* **751**, 76 (2012).
34. M. J. Mumma, S. B. Charnley, *Annu. Rev. Astron. Astrophys.* **49**, 471–524 (2011).

Acknowledgments: We are grateful to S. Schnee for data calibration and reduction assistance. C.Q. thanks the Smithsonian Astrophysical Observatory (SAO) Radio Telescope Data Center (RTDC) staff for their generous computational support. C.Q., K.I.O., and D.J.W. acknowledge grant NNX11AK63 from NASA Origins of Solar Systems. P.D. acknowledges a grant from Programa de Apoyo a Proyectos de Investigación e Innovación Tecnológica–UNAM. E.B. acknowledges support from NSF grant 1008800. This Report makes use of the following ALMA data: ADS JAO. ALMA#2011.0.00340.S. ALMA is a partnership of the European Southern Observatory (ESO) (representing its member states), NSF (USA), and the National Institute of Natural Sciences (Japan), together with the National Research Council (Canada) and the National Science Council and Academia Sinica's Institute of Astronomy and Astrophysics (ASIAA) (Taiwan), in cooperation with the Republic of Chile. The Joint ALMA Observatory is operated by ESO, Associated Universities, Inc. (AUI)/National Radio Astronomy Observatory, and the National Astronomical Observatory of Japan. We also make use of the Submillimeter Array (SMA) data: project #2004-214 (principal investigator, C.Q.). The SMA is a joint project between SAO and ASIAA and is funded by the Smithsonian Institution and the Academia Sinica.

Supplementary Materials

www.sciencemag.org/cgi/content/full/science.1239560/DC1
Materials and Methods
Figs. S1 to S5
Tables S1 to S3
References (*35*–*52*)

23 April 2013; accepted 2 July 2013
Published online 18 July 2013;
10.1126/science.1239560

A Quantum Many-Body Spin System in an Optical Lattice Clock

M. J. Martin,[1,2]*† M. Bishof,[1,2] M. D. Swallows,[1,2]‡ X. Zhang,[1,2] C. Benko,[1,2] J. von-Stecher,[1,2]§ A. V. Gorshkov,[3] A. M. Rey,[1,2]† Jun Ye[1,2]†

Strongly interacting quantum many-body systems arise in many areas of physics, but their complexity generally precludes exact solutions to their dynamics. We explored a strongly interacting two-level system formed by the clock states in ^{87}Sr as a laboratory for the study of quantum many-body effects. Our collective spin measurements reveal signatures of the development of many-body correlations during the dynamical evolution. We derived a many-body Hamiltonian that describes the experimental observation of atomic spin coherence decay, density-dependent frequency shifts, severely distorted lineshapes, and correlated spin noise. These investigations open the door to further explorations of quantum many-body effects and entanglement through use of highly coherent and precisely controlled optical lattice clocks.

Strongly correlated quantum many-body systems have become a major focus of modern science. Researchers are using quantum-degenerate atomic gases (*1*–*6*), ultracold polar molecules (*7*–*9*), and ensembles of trapped ions (*10*, *11*) to realize previously unidentified quantum phases of matter and simulate complex condensed matter systems. Another prom-